Microporous Networks of High-Performance Polymers: Elastic Deformations and Gas Sorption Properties

Jens Weber, Markus Antonietti, and Arne Thomas*

Max-Planck-Institute of Colloids and Interfaces, Department of Colloid Chemistry, Research Campus Golm, D-14424 Potsdam, Germany

Received November 13, 2007; Revised Manuscript Received January 24, 2008

ABSTRACT: Aromatic poly(imide) and poly(amide) networks have been synthesized using a tetrafunctionalized spirobifluorene unit as cross-linker and packing inhibitor. The poly(imide) network exhibits intrinsic microporosity and consequently high surface areas of about 1000 m^2/g from nitrogen sorption, while the poly(amide) network does not exhibit N_2-accessible pores and consequently no detectable surface area. Combined gas sorption and small-angle X-ray scattering analysis reveals the particularities for the evaluation of pore volume, pore size distribution, and surface areas of such soft microporous frameworks. Besides surface adsorption, pronounced elastic deformation is observed during increasing gas pressures, related to inner gas binding sites also known from the "dual-mode sorption" process of classical polymer membranes. The networks have furthermore been tested as hydrogen storage materials and show high hydrogen uptakes at low pressures. Surprisingly, also the polyamide network stored remarkable amounts of hydrogen.

Introduction

Organic materials, which resemble the structure of well-known microporous inorganic materials (activated carbons, zeolites), provide new opportunities in emerging technological areas. For example, materials with tunable pore size and high surface areas can be envisaged, which allow an exquisite control over the chemical nature of their large accessible surface areas as well as the physical properties of the resulting networks. A wide variety of possible functionalities (acid/base, aromatic, hydrophilic/hydrophobic, chiral, and so on) can be imagined to be part of the pore walls, which cannot be accessed for inorganic materials. Research in this direction can furthermore yield functional materials exhibiting low dielectric constant and refractive index as well as low heat conductivity together with attractive mechanical properties, as for example ductility and elasticity. In addition, materials based only on light elements are advantageous in applications where specific weight must be kept at a minimum (e.g., hydrogen storage for transportation applications).

In our opinion, three types of microporous organic materials can be distinguished referring to the recent literature: Besides the well-described hyper-cross-linked resins introduced by Davankov et al.,[1,2] a new class of porous covalent organic frameworks (COF) has been recently presented by Côte, Yaghi, and co-workers.[3–5] A third type of microporous organic materials are polymers with intrinsic microporosity, introduced by Budd, McKeown, and co-workers.[6–8] The main feature of the latter polymers is a packing-breaking monomer architecture (e.g., stiff units with a spiro-center) introduced into otherwise rigid linear polymer chains. Thus, polymers with highly rigid and contorted molecular structures result, which prevent space-efficient packing in the solid state and consequently exhibit microporosity. So far, this concept was successfully employed for ladder-type polymers made via dioxane-forming polymerization, only. Recently, we expanded this concept toward soluble poly(amide) and poly(imide) using monomers derived from 9,9′-spirobifluorene.[9] A comparison of the measured microporosity of the more rigid poly(imide) with the structurally closely related, but more flexible, poly(amide)s suggested that the overall rigidity of the polymers might be the key factor for controlling intrinsic microporosity.

Herein we present the synthesis and characterization of various poly(amide) and poly(imide) networks, based on a spirobifluorene derivative. These networks are analyzed by means of scanning electron microscopy, infrared spectroscopy, gas sorption, and small-angle X-ray scattering (SAXS), revealing the appearance of intrinsic microporosity in the one case but not in the other. Because of their low density and high surface areas, microporous polymers have been described as a promising material for hydrogen storage applications.[10–15] The low-pressure hydrogen sorption properties of the spirobifluorene-based networks will be discussed. However, the gas sorption properties of these materials are still not completely understood. Especially, swelling effects or elastic deformations have to be taken into account during gas sorption,[16] as polymeric materials are rather soft compared to their inorganic counterparts. For metal−organic frameworks a breathing phenomenon, i.e., a topological rearrangement of the network, was described upon the inclusion of gas or solvent molecules into their structures.[17,18] Herein we report that microstructural changes of microporous polymer networks can occur even at low pressure.

Experimental Section

Details of the synthesis of monomer **1** and the instrumental methods can be found in the Supporting Information.

Synthesis of Poly(amide) PA1. PA1 was synthesized by a modified Yamazaki method using triphenyl phosphite as condensation catalyst.[19] A mixture of **1** (0.200 g, 0.531 mmol) and terephthalic acid (**2**) (0.177 g, 1.06 mmol) was dissolved in 0.5 mL of dry NMP containing 0.05 mL of dry pyridine. The solution was heated to 150 °C under an argon atmosphere. After reaching the desired temperature TPP (0.5 mL) is added, and the reaction was conducted for 6 h.

Synthesis of Poly(amide) PA2. 0.200 g (0.531 mmol) of **1** was dissolved in 2 mL of dry NMP. 1,3,5-Benzenetricarboxylic acid trichloride (**4**) (0.188 g, 0.708 mmol) was added, and the mixture was stirred at room temperature for 0.5 h under an argon atmosphere. Afterward, the temperature was raised to 80 °C and the mixture was stirred for an additional hour. Finally, the mixture was heated to 150 °C and kept for 4 h at 150 °C.

Synthesis of Poly(imide) PI1. 0.200 g (0.531 mmol) of **1** was dissolved in 2 mL of freshly distilled *m*-cresol. 0.232 g (1.06 mmol)

* Corresponding author. E-mail: arne.thomas@mpikg.mpg.de.

10.1021/ma702495r CCC: $40.75
Published on Web 03/19/2008

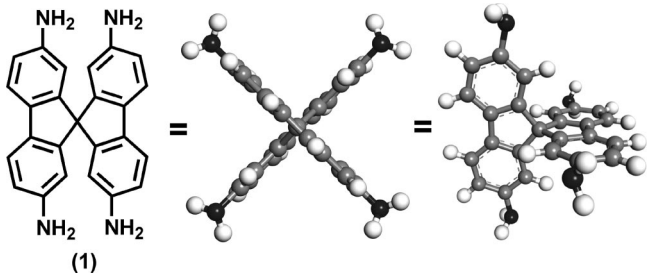

Figure 1. Chemical structure of 2,2′,7,7′-tetraamino-9,9′-spirobifluorene (**1**) and two views on its three-dimensional structure.

of pyromellitic acid dianhydride (**3**) and 3 drops of isoquinoline were added, and the mixture was stirred at room temperature for 1 h under an argon atmosphere. Afterward, the temperature was raised to 80 °C, and the mixture was stirred for an additional hour. To complete the reaction, the mixture was heated to 200 °C for 5 h.

Synthesis of Poly(imide) PI2. 0.114 g (0.531 mmol) of 3,3′-diaminobenzidine (**5**) was dissolved in 2 mL of freshly distilled *m*-cresol. 0.232 g (1.06 mmol) of pyromellitic acid dianhydride (**3**) and 3 drops of isoquinoline were added, and the mixture was stirred at room temperature for 1 h under an argon atmosphere. Afterward, the temperature was raised to 80 °C, and the mixture was stirred for an additional hour. To complete the reaction, the mixture was heated to 200 °C for 5 h.

Purification of the Polymer Networks. All gels were purified as follows: After cooling to room temperature the gel was stirred in DMF overnight. The solvent was removed by centrifugation, and the crude gel was again stirred in DMF for 4 h. After removal of the DMF, the gel was extensively washed with acetone and dried in vacuo.

Methods. The NMR measurements were conducted on a Bruker DPX-400 spectrometer operating at 400.1 MHz. The IR spectra were collected with a BIORAD FTS 6000 FTIR spectrometer, equipped with an attenuated total reflection (ATR) setup. Nitrogen sorption experiments were conducted at 77 K using a Micromeritics Tristar 3000 automated gas adsorption analyzer. Micropore analyses and Krypton sorption experiments were carried out at 77 K using Autosorb-1 from Quantachrome Instruments. Before sorption measurements, the samples were degassed in vacuo overnight at 150 °C. Wide-angle scattering was performed using a D8 diffractometer from Bruker Instruments (wavelength 0.154 nm). Small-angle X-ray scattering was performed on a Kratky camera from Anton Paar Instruments (wavelength 0.154 nm). Scattering data are reported with the scattering vector s being defined as $s = 2\sin(\theta)/\lambda$, where θ is the scattering angle and λ is the wavelength of the X-rays.

Results and Discussion

Spirobifluorene has been previously applied as a structure directing motif for porous hydrogen-bonded networks[20,21] and organic optoelectronic materials.[22–24] As spirobifluorene is a bulky and rigid structural unit, its incorporation into polymer networks is also expected to yield in packing defects and a high amount of free volume up to the appearance of accessible microporosity. 2,2′,7,7′-Tetraminospirobifluorene (**1**) was used as the structure directing motif for the generation of several poly(amide) and poly(imide) networks. The synthesis of **1** was performed following known protocols.[20,25] The chemical structure of **1** is depicted in Figure 1 together with a three-dimensional model of its structure. The model shows the crosslike spatial orientation of reactive amine groups which predefines the polymer structure.

The poly(amide) network **PA1** was synthesized by polycondensation of **1** with terephthalic acid (**2**) using a modified Yamazaki protocol. Reaction of **1** with benzene-1,3,5-tricarboxylic acid trichloride (**4**) gave the polyamide **PA2**. A spirobifluorene-based poly(imide) network (**PI1**) was synthesized with **1** and pyromellitic acid dianhydride (**3**). For comparison, a similar polycondensation was carried out, however, using 3,3′-diaminobenzidine (**5**) as the amino compound (**PI2**). The chemical structures of the applied monomers and the resulting polymer networks are summarized in Figure 2.

For all polycondensation reactions almost quantitative yields of the products were observed, pointing toward a high degree of polymerization. Furthermore, a high degree of condensation can be assumed from infrared spectroscopy, as e.g. in the polyimide networks the OH and NH vibrational modes of the monomers have completely vanished (Figure S1 of the Supporting Information).

The nitrogen sorption measurements revealed no microporosity for the poly(amide) network **PA1** ($S_{BET} = 50\ m^2\ g^{-1}$), while the poly(imide) network **PI1** exhibits a pronounced microporosity with a BET surface area of 982 $m^2\ g^{-1}$ and a pore volume of 0.62 $cm^3\ g^{-1}$ at $p/p_0 = 0.9$. It is worth underlining that these high values were reached without addition of a selected porogen; i.e., this microporosity is indeed intrinsic and due to the structure of the polymer.[26]

Although amide bonds in a polymer chain are regarded as rather rigid moieties, they are definitely more adaptable then imide linkages.[27] The preservation of porosity in polymer networks can be achieved by adding additional cross-linkers to their synthesis, thus hardening the polymer network.[28] To increase the stiffness of the polyamide network, 1,3,5-benzenetricarboxylic acid trichloride (**4**) was used as a comonomer to achieve a higher cross-linking density in the polyamide network **PA2** (Figure 2b). However, from nitrogen sorption measurements this highly cross-linked polymer network exhibited no observable porosity ($S_{BET} = 0\ m^2\ g^{-1}$). The usage of the acid chloride **4** also allowed the use of reaction conditions that are comparable to those used for the synthesis of the polyimide networks. The reaction conditions applied in the Yamazaki-type synthesis of the poly(amide) networks are rather different from those used for the poly(imide) synthesis, and from scanning electron microscopy measurements it can be observed that this difference leads to different micromorphologies (see Figure S2). The synthetic pathways toward the poly(imide) networks and the polyamide **PA2** give rise to an early phase separation resulting in a disrupted morphology. In contrast, the gel formation in the Yamazaki-type reaction toward **PA1** proceeds smoothly and results in more homogeneous gel morphology, yielding in a plain, filmlike morphology above the scale of micrometers, while below this scale, the film expresses considerable surface texture. This obvious textural porosity is again observed in the nitrogen sorption measurements as macropororosity and outer surface area. Therefore, it can be concluded that the reaction pathway has no influence on the occurrence of intrinsic microporosity.

At last, to prove the necessity of a packing-breaking motif as a prerequisite for intrinsic microporosity, a reference poly(imide) network without tetraaminospirofluorene (**1**), but 3,3′-diaminobenzidine (**5**) as a cross-linker, was synthesized (Figure 2c, **PI2**) and compared to the spirobifluorene-derived **PI1**. No microporosity could be observed for **PI2** ($S_{BET} = 19\ m^2\ g^{-1}$), although it showed the same macroscopic morphology as **PI1**, proving the crucial influence of the contorted architecture of the spirobifluorene motif.

Summarizing these results, the low surface areas found for **PA1** and **PI2** can be attributed to the presence of macropores and surface texture, while they are obviously not related to inherent microporosity, and only **PI1** exhibits a high surface area, attributable to a pronounced microporosity. (Additionally performed krypton sorption measurements even yield a BET surface area of 1280 $m^2\ g^{-1}$ for sample **PI1**.) The reference

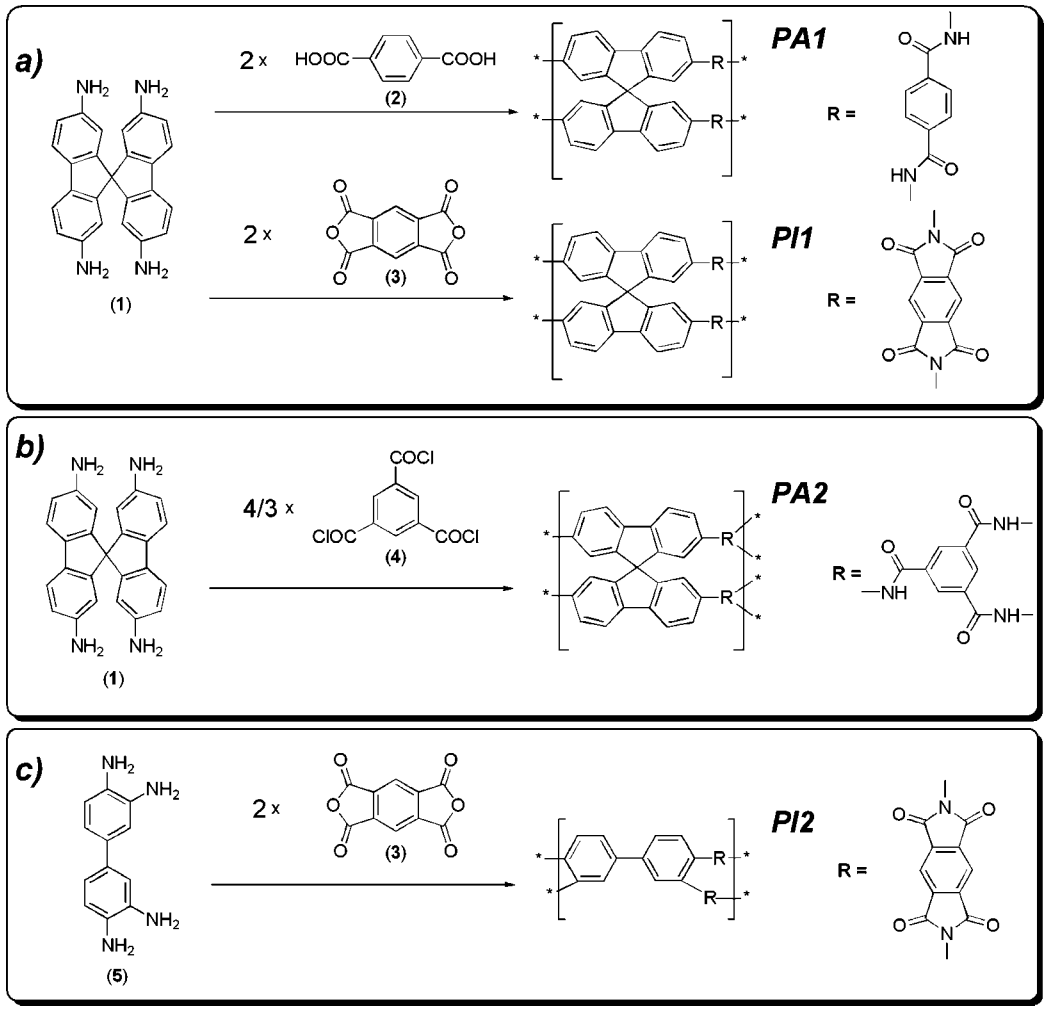

Figure 2. (a) Synthetic pathway toward the poly(amide) network **PA1** and the poly(imide) network **PI1** and the characteristic chemical structures of poly(amide)s and poly(imide)s. (b) Synthesis of **PA2**. (c) Synthesis of **PI2**.

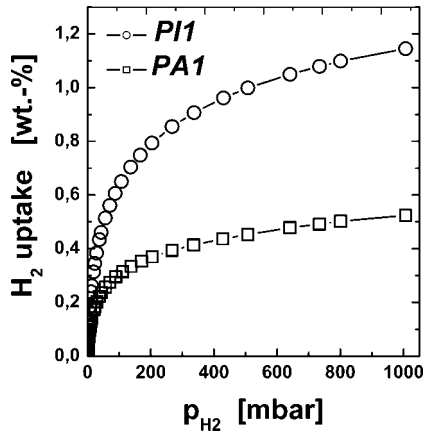

Figure 3. Hydrogen sorption measurements on the polymer networks **PA1** and **PI1**, performed at 77 K.

examples show that the intrinsic microporosity of such polymer networks, detectable via N_2 sorption, indeed primarily depends on the molecular architecture of the respective material and not on the applied reaction conditions.

Microporous polymers are regarded as potential hydrogen storage materials due to their low density and their very promising high gravimetric storage capacity.[10–15] Figure 3 presents the results of low-pressure hydrogen sorption measurements of **PA1** and **PI1** at 77 K. **PI1** shows a very good hydrogen uptake at low pressures. The uptake of 1.15 wt % at 1 bar is comparable to those found for other microporous polymers.[12] Intriguingly, even though no pronounced nitrogen uptake was observed for **PA1**, also this polymer showed a significant hydrogen uptake of 0.52 wt %. Such selective gas sorption properties were also reported for some metal−organic frameworks and attributed to size exclusion effects, that is, to small micropore dimensions, which can accommodate smaller gas molecules but exclude molecules with larger kinetic diameters.[29–32]

Both small-angle X-ray scattering (SAXS) and wide-angle X-ray scattering (WAXS) experiments were applied to achieve a detailed insight into the polymer microstructure. WAXS experiments confirmed that all networks are of amorphous nature, which is in accordance with results obtained on soluble microporous poly(amide)s and poly(imide)s[9] (see Figure S3). Small-angle scattering turned out to be a powerful tool to reveal structural details of activated carbons,[33] but there is no experience for microporous polymer networks up to now. Therefore, pressure-dependent SAXS experiments were performed at room temperature. The samples were first measured under vacuum and second in a helium atmosphere at ambient pressure to investigate possible swelling effects and elastic deformations. Figure 4 shows the as-measured scattering patterns of **PI1** and **PA1** under both conditions.

Both samples show rather high X-ray scattering and a pronounced increase of scattering intensity toward small scattering vectors, characteristic for high surface area systems and

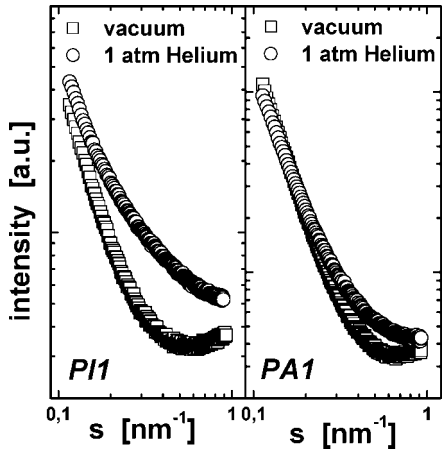

Figure 4. SAXS patterns of **PI1** and **PA1** measured at room temperature under vacuum and helium atmosphere at ambient pressures, respectively.

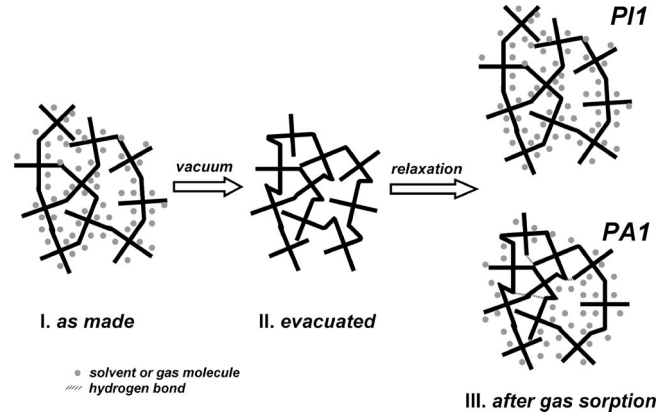

Figure 5. Schematic drawing of the suggested deformation−relaxation process during evacuation and gas sorption: (I) As-made networks contain residual solvent or gas molecules. (II) Upon evacuation the solvent/gas molecules are removed and the networks are contracted, involving deformation of chains and bonds. (III) By the uptake of gas molecules the network can relax again (**PI1**); if this process is not restricted by intermolecular interactions just as hydrogen bonding (**PA1**).

the presence of larger structures within the polymer films. These finding is in accordance with the results from nitrogen sorption at high relative pressures and the electron micrographs. The SAXS patterns of the networks with and without helium mainly differ at scattering vectors larger than 0.2 nm^{-1}, corresponding to length scales of 5 nm and below. This can be interpreted as evidence for pressure-dependent structural changes. While we observe a continuous decay of the scattering intensity $I(s)$ under a helium atmosphere, which turns out to be Porod behavior (see below), we observe an increase of $I(s)$ at high scattering vectors under vacuum. This can be interpreted as the onset of a Bragg peak, originating from liquidlike ordered, compressed pores.

However, we have not been able to determine the magnitude of the deformation yet. In contrast to metal− organic frameworks, which can be analyzed by means of classic crystallography, this is not easily possible for the amorphous polymers.

Since the SAXS pattern of **PA1** under vacuum is not too different from that of **PI1**, it can be concluded that the fundamental difference between both samples is found in the course of the pressure change from vacuum toward the helium atmosphere. It is known that microporous materials, especially those with pores of subnanometer dimension, can adsorb significant amounts of helium even at room temperature.[34,35] Therefore, an explanation of the pressure-dependent changes in the scattering patterns must regard (i) the physisorption of helium and (ii) the possibility of elastic deformations. It is well-known that even stiff microporous materials, as for example zeolites or activated carbon, are prone to pressure-dependent deformations.[16,36–38]

Assuming that the polymer networks are compressed upon solvent removal in order to minimize the interfacial tension, deformation of bonds and bond angles takes place; i.e., mechanical stress is induced. The total free energy of the system is therefore balanced by the contributions of the interfacial force and elastic forces. Physisorption of gases can potentially reduce the interfacial tension, leading to relaxation of the polymer network. In the case of **PI1** this relaxation leads to the observation of microporosity. For **PA1** also hydrogen bonding has to be regarded, which is proved by infrared spectroscopy (see Figure S1). It can be speculated that hydrogen bonds suppress the full relaxation of the network, explaining the lower surface area and the difference observed in the SAXS patterns. The deformation−relaxation phenomenon is schematically depicted in Figure 5.

SAXS is able to detect the inner interface of the system, which cannot be accessed by nitrogen sorption experiments, and it is possible to quantify the SAXS data, allowing the calculation of specific surface areas and average pore sizes. The measured scattering curve $I(s)$ were corrected for the smearing due to the presence of three-dimensional electron density fluctuations, which are due to the atomic heterogeneity within the polymer.[39] Their subtraction from the scattering curves reveals a pattern, which is then only dependent on the morphology of the two-phase system (see Figure S4).

PI1 shows well-defined Porod behavior allowing the calculation of the Porod length l_p, which is a characteristic length of the system.[40] A Porod length l_p of 0.96 nm was determined, a value which is reasonable for a microporous polymer. In contrast to the polyimide networks, the Porod behavior found for the polyamide networks, e.g., **PA1** is less defined. However, it is possible to determine the Porod length to $l_p = 1.74$ nm.

The Porod length is related to the interface of a two-phase system, i.e., to the specific surface of the microporous material by the equation

$$\frac{S}{V} = \frac{4\varphi(1-\varphi)}{l_p} \quad (1)$$

Thus, to calculate the surface area just an estimate for the relative volume fraction of pores is needed. The porosity φ is the volume fraction of the pores that can be calculated from the pore volume determined by nitrogen sorption and the volume occupied by the polymer chains. It was suggested by Tsyurupa and Davankov that the specific volume of the polymer chain can be calculated from the van der Waals volume and the molecular weight of the repeating unit.[41] The van der Waals volume of the polymers was determined with molecular modeling using the COMPASS forcefield implemented within the FORCITE module of the Materials Studio Modeling Software 3.1 (see Table T1 and Figure S5). On the basis of this method, the porosity of **PI1** and **PA1** was determined to 0.56 and 0.23, respectively. It should be underlined that this pore volume is calculated on the basis of packing; i.e., it is not necessarily assessable by nitrogen sorption, especially in case of **PA1**.

With these values, SAXS quantifies the specific surface area of the helium-filled **PI1** to 1130 m^2 g^{-1}. This value is in good agreement with the results from N_2 (982 m^2 g^{-1}) and Kr sorption measurements (1280 m^2 g^{-1}). The number-average pore size determined by SAXS is 2.2 nm.

In contrast to the sorption measurements, the SAXS measurements also yield a significant specific surface area of 280 m^2 g^{-1} for **PA1**. However, because of the error of the uncertain

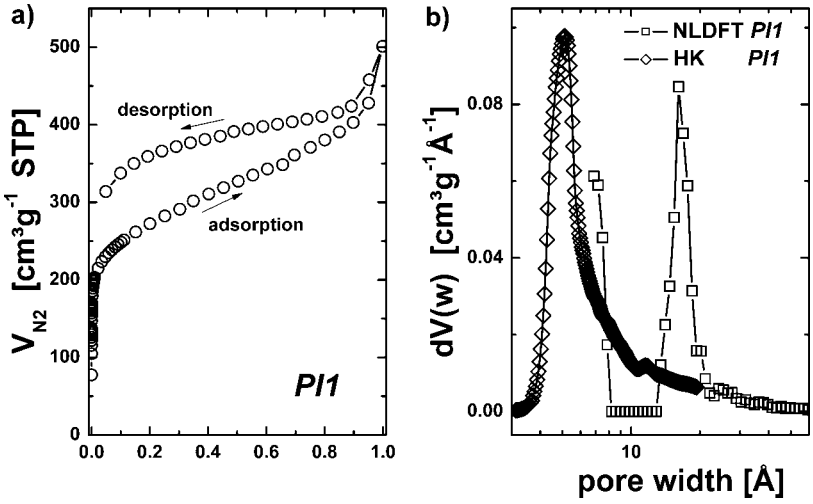

Figure 6. (a) Nitrogen sorption isotherm of **PI1**. (b) Comparison of the micropore analysis data derived from the HK and NLDFT model. NLDFT analysis is based on the assumption of the adsorbent having surface properties as activated carbon.

pore volume for this polymer network, a more than semiquantitative analysis of these measurements is to some point questionable.

The evidence of pressure-dependent structural changes which take place during the gas sorption process allows an explanation for the particularities often observed for porous polymer networks during low-temperature nitrogen sorption. Here it is frequently observed that the desorption branch of the isotherm does not close to the adsorption branch at low relative pressures (Figure 6). This behavior is mostly attributed to a swelling of the polymer matrix, but so far no detailed explanation for this phenomenon has been given. Most probably, this effect can be described by a similar process as observed in ordinary (i.e., nonporous) polymer films and membranes at high-pressure gas permeation experiments, called dual-mode sorption.[42] The dual-mode sorption model assumes the existence of a fractional free volume of pores within polymer films, which can be filled by gas molecules at first ("pocket filling"), while there is an additional Henry sorption within the film, which is proportional to the gas pressure ("swelling").

For microporous systems, after filling of the micropores at low relative pressures, a continuous further uptake of gas molecules can be seen with increasing, but still moderate, relative pressures. This can be explained by calculating the capillary pressure in the micropores via the Young−Laplace equation, yielding values of up to 100 bar. That means that the frequently described "swelling" of soft microporous materials during the process of nitrogen sorption might be closely related to process of Henry sorption described in the classical dual sorption model of membranes. This type of sorption is then seen in the adsorption isotherm, which is constantly rising also after the micropores are filled and the hysteresis between the adsorption and desorption branch of the nitrogen sorption measurement, which do not close a lower partial pressures (Figure 6).

This effect has also a strong impact on the determination of the pore size distribution (PSD) from the nitrogen sorption isotherm. Figure 6 shows the PSD determined by applying a non local density functional theory (NLDFT) model and the Horvarth−Kawazoe (HK) model. It is obvious that both models give contrary results. While the HK method predicts ultramicropores (pore width <0.8 nm) to be the dominant species, the NLDFT model differentiates between ultramicropores and supermicropores (pore width >0.8 nm), showing that care is advised applying either of these methods uncritically on soft, organic microporous materials.

In conclusion, novel poly(amide) and poly(imide) networks were synthesized, incorporating spirobifluorene as cross-linker and structure-breaking motif into the polymer chains. Variation of the synthesis conditions and the introduction of other cross-linkers into the networks proved that the observed intrinsic microporosity indeed mainly depends on the molecular architecture of the respective material.

Further information on the structure of the polymer networks was obtained from SAXS measurements, performed at vacuum and ambient helium pressures. Structural changes upon evacuation were observed. We suggest a compression of the networks upon evacuation. Upon changing the pressure to ambient conditions, a relaxation of the networks is proposed to happen. It is likely that the relaxation process is accompanied by the sorption of gases.

The relaxation of the networks might be hindered if a secondary interaction like hydrogen bonding takes place in the deformed state. This might lead to the presence of very small micropores and can explain the hydrogen sorption properties of **PA1**. The knowledge of this phenomenon can furthermore be crucial for the identification of other potentially microporous polymers.

It must be stated that our explanation of the phenomenon is a suggestion and has to be verified by future experiments on these polymers as well as on other known microporous polymers. Especially the amount of helium adsorbed within the networks has to be quantified. Also, it is necessary to determine the amount of deformation. Combinations of SAXS, gas sorption experiments, and dilatometric measurements seem promising to answer the open questions regarding the process of elastic deformations.

The observation of the deformations points to a low-temperature gas sorption mechanism known as "dual-mode sorption" for nonporous polymers. That this process occurs in microporous polymers even at low outer pressures is presumably supported by the high capillary pressure within the pores, which obviously equilibrates through the nanodimensions within the polymer network to act also in the bulk of the polymer. Therefore, care must be taken in the analysis of the porosity features (e.g., the pore size distribution) of microporous "soft" materials by nitrogen sorption.

Acknowledgment. Financial support from ENERCHEM is gratefully acknowledged. We thank Dr. Jens Assmann, Dr. Markus Schubert, Dr. Jianhua Ba, and the BASF AG for the hydrogen sorption experiments.

Supporting Information Available: Details of synthesis of monomer **1** and instrumental methods. This material is available free of charge via the Internet at http://pubs.acs.org.

References and Notes

(1) Davankov, V. A.; Tsyurupa, M. P. *React. Polym.* **1990**, *13* (1–2), 27–42.
(2) Tsyurupa, M. P.; Davankov, V. A. *React. Funct. Polym.* **2002**, *53* (2–3), 193–203.
(3) Cote, A. P.; Benin, A. I.; Ockwig, N. W.; O'Keeffe, M.; Matzger, A. J.; Yaghi, O. M. *Science* **2005**, *310* (5751), 1166–1170.
(4) Tilford, R. W.; Gemmill, W. R.; zur Loye, H. C.; Lavigne, J. J. *Chem. Mater.* **2006**, *18* (22), 5296–5301.
(5) El-Kaderi, H. M.; Hunt, J. R.; Mendoza-Cortes, J. L.; Cote, A. P.; Taylor, R. E.; O'Keeffe, M.; Yaghi, O. M. *Science* **2007**, *316* (5822), 268–272.
(6) McKeown, N. B.; Hanif, S.; Msayib, K.; Tattershall, C. E.; Budd, P. M. *Chem. Commun.* **2002**, (23), 2782–2783.
(7) McKeown, N. B.; Makhseed, S.; Budd, P. M. *Chem. Commun.* **2002**, (23), 2780–2781.
(8) Budd, P. M.; Ghanem, B. S.; Makhseed, S.; McKeown, N. B.; Msayib, K. J.; Tattershall, C. E. *Chem. Commun.* **2004**, (2), 230–231.
(9) Weber, J.; Antonietti, M.; Thomas, A. *Macromol. Rapid Commun.* **2007**, (18–19), 1871–1876.
(10) McKeown, N. B.; Budd, P. M.; Book, D. *Macromol. Rapid Commun.* **2007**, *28* (9), 995–1002.
(11) Budd, P. M.; Butler, A.; Selbie, J.; Mahmood, K.; McKeown, N. B.; Ghanem, B.; Msayib, K.; Book, D.; Walton, A. *Phys. Chem. Chem. Phys.* **2007**, *9* (15), 1802–1808.
(12) Wood, C. D.; Tan, B.; Trewin, A.; Niu, H. J.; Bradshaw, D.; Rosseinsky, M. J.; Khimyak, Y. Z.; Campbell, N. L.; Kirk, R.; Stockel, E.; Cooper, A. I. *Chem. Mater.* **2007**, *19* (8), 2034–2048.
(13) Lee, J. Y.; Wood, C. D.; Bradshaw, D.; Rosseinsky, M. J.; Cooper, A. I. *Chem. Commun.* **2006**, (25), 2670–2672.
(14) Ahn, J. H.; Jang, J. E.; Oh, C. G.; Ihm, S. K.; Cortez, J.; Sherrington, D. C. *Macromolecules* **2006**, *39* (2), 627–632.
(15) Germain, J.; Hradil, J.; Frechet, J. M. J.; Svec, F. *Chem. Mater.* **2006**, *18* (18), 4430–4435.
(16) Fomkin, A. A. *Adsorption* **2005**, *11* (3–4), 425–436.
(17) Bourrelly, S.; Llewellyn, P. L.; Serre, C.; Millange, F.; Loiseau, T.; Ferey, G. *J. Am. Chem. Soc.* **2005**, *127* (39), 13519–13521.
(18) Serre, C.; Mellot-Draznieks, C.; Surble, S.; Audebrand, N.; Filinchuk, Y.; Ferey, G. *Science* **2007**, *315* (5820), 1828–1831.
(19) Yamazaki, N.; Matsumoto, M.; Higashi, F. *J. Polym. Sci., Part A: Polym. Chem.* **1975**, *13* (6), 1373–1380.
(20) Fournier, J. H.; Maris, T.; Wuest, J. D. *J. Org. Chem.* **2004**, *69* (6), 1762–1775.
(21) Demers, E.; Maris, T.; Wuest, J. D. *Cryst. Growth Des.* **2005**, *5* (3), 1227–1235.
(22) Marsitzky, D.; Murray, J.; Scott, C.; Carter, K. R. *Chem. Mater.* **2001**, *13* (11), 4285–4289.
(23) Johansson, N.; dosSantos, D. A.; Guo, S.; Cornil, J.; Fahlman, M.; Salbeck, J.; Schenk, H.; Arwin, H.; Bredas, J. L.; Salanek, W. R. *J. Chem. Phys.* **1997**, *107* (7), 2542–2549.
(24) Saragi, T. P. I.; Spehr, T.; Siebert, A.; Fuhrmann-Lieker, T.; Salbeck, J. *Chem. Rev.* **2007**, *107* (4), 1011–1065.
(25) Thiemann, F.; Piehler, T.; Haase, D.; Saak, W.; Lutzen, A. *Eur. J. Org. Chem.* **2005**, (10), 1991–2001.
(26) McKeown, N. B.; Budd, P. M.; Msayib, K. J.; Ghanem, B. S.; Kingston, H. J.; Tattershall, C. E.; Makhseed, S.; Reynolds, K. J.; Fritsch, D. *Chem.—Eur. J.* **2005**, *11* (9), 2610–2620.
(27) Aharoni, S. M.; Edwards, S. F. *Macromolecules* **1989**, *22* (8), 3361–3374.
(28) Weber, J.; Antonietti, M.; Thomas, A. *Macromolecules* **2007**, *40* (4), 1299–1304.
(29) Chen, B. L.; Ma, S. Q.; Hurtado, E. J.; Lobkovsky, E. B.; Liang, C. D.; Zhu, H. G.; Dai, S. *Inorg. Chem.* **2007**, *46* (21), 8705–8709.
(30) Dinca, M.; Long, J. R. *J. Am. Chem. Soc.* **2005**, *127* (26), 9376–9377.
(31) Dybtsev, D. N.; Chun, H.; Yoon, S. H.; Kim, D.; Kim, K. *J. Am. Chem. Soc.* **2004**, *126* (1), 32–33.
(32) Ma, S. Q.; Sun, D. F.; Wang, X. S.; Zhou, H. C. *Angew. Chem., Int. Ed.* **2007**, *46* (14), 2458–2462.
(33) Smarsly, B.; Antonietti, M.; Wolff, T. *J. Chem. Phys.* **2002**, *116* (6), 2618–2627.
(34) Maggs, F. A. P.; Schwabe, P. H.; Williams, J. H. *Nature (London)* **1960**, *186* (4729), 956–958.
(35) Neimark, A. V.; Ravikovitch, P. I. *Langmuir* **1997**, *13* (19), 5148–5160.
(36) Ravikovitch, P. I.; Neimark, A. V. *Langmuir* **2006**, *22* (26), 10864–10868.
(37) Reichenauer, G.; Scherer, G. W. *J. Non-Cryst. Solids* **2000**, *277* (2–3), 162–172.
(38) Yakovlev, V. Y.; Fomkin, A. A.; Tvardovski, A. V. *J. Colloid Interface Sci.* **2003**, *268* (1), 33–36.
(39) Perret, R.; Ruland, W. *Kolloid Z. Z. Polym.* **1971**, *247* (1–2), 835.
(40) Glatter, O.; Katky, O. *Small Angle X-Ray Scattering*; Academic Press: New York, 1982.
(41) Tsyurupa, M. P.; Davankov, V. A. *React. Funct. Polym.* **2006**, *66* (7), 768–779.
(42) Tsujita, Y. *Prog. Polym. Sci.* **2003**, *28* (9), 1377–1401.

MA702495R